To Storm or Not to Storm: Measurement Method to Quantify Impact of Exterior Envelope Airtightness on Energy Usage Prior to Construction

André O. Desjarlais **Kenneth W. Childs, P.E.** **Jeffrey E. Christian**
Member ASHRAE

ABSTRACT

The purpose of this project was to devise a simple, experimentally validated method for quantifying the energy impacts of exterior envelope air leakage. Four full-size exterior envelope test specimens, two opaque wall systems and two fenestration systems, were built for determining simultaneous conductive and convective heat loss. The two opaque clear wall sections were metal-faced sandwich panel and cold formed steel frame. The steel frame system was a conventional lightweight cold formed steel-framed wall tested before and after foam air-sealing in the cavity prior to installing conventional fiberglass batts. The second opaque wall system was a metal panel system, which is used for commercial cold storage facilities as well as exterior curtain walls for multifamily residential and commercial buildings. The window systems were tested for energy loss both with and without the addition of storm windows. The measurements were made in a specially modified guarded hot box that can maintain both heat and mass flow across the test specimen. Thus, both heat and mass flow were measured. A proposed methodology for taking data from hot box tests and deriving a simple design tool suitable for inclusion in a simplified prediction tool (instrument) is presented, and the methodology is tested with data from the hot box measurements. Further envelope tests will be required since the limited number of systems tested are not sufficient to confirm the applicability of the proposed methodology. At this time the method has only been applied to a few different types of windows. The paper concludes that the methodology developed for quantifying the airtightness for windows is promising and proposes that additional opaque wall details be laboratory tested and the methodology expanded to the entire exterior envelope.

INTRODUCTION

The purpose of this International Energy Agency (IEA) Annex 32 project is to devise a simple, experimentally validated method for quantifying the annual energy impacts of exterior envelope air leakage paths. This was identified in the April 1997 IEA Annex 32 meeting at Oak Ridge as a gap in the available tools for verifying the functional requirement C 4.2 airtightness of the building envelope (Integral client's brief, functional descriptions, September 1997). The project was sponsored by the State and Community Programs Office of the U.S. Department of Energy. The final goal is to develop and implement this method into a simplified software prediction tool.

The cold formed steel-frame wall was built without any particular air control provisions. This clear wall test specimen was built with an anticipated air passage between two adjoining sheathing sheets on the exterior surface and an electrical outlet and switch box penetrating the interior drywall sheathing. The experimental plan called for airtightness measurements before and after the application of sprayed polyurethane foam insulation installed in the wall cavities prior to attaching the interior drywall. However, airtightness measurements made prior to the installation of the foam revealed an airtight system even with pressures across the wall exceeding 75 pascals. It appears that when these wall systems are assembled with some degree of care, they can be built initially with very low air permeability. The second opaque wall system, which consisted of metal-faced sandwich panels, had two 2.4 m (8 ft) panel to panel joints. This wall system was found to permit some air movement through the seams.

In order to quantify the effect of exterior envelope airtightness across the windows on energy usage, a series of energy

André O. Desjarlais is a program manager, **Kenneth W. Childs** is a group leader, and **Jeffrey E. Christian** is director of the Buildings Technology Center at Oak Ridge National Laboratory, Oak Ridge, Tenn.

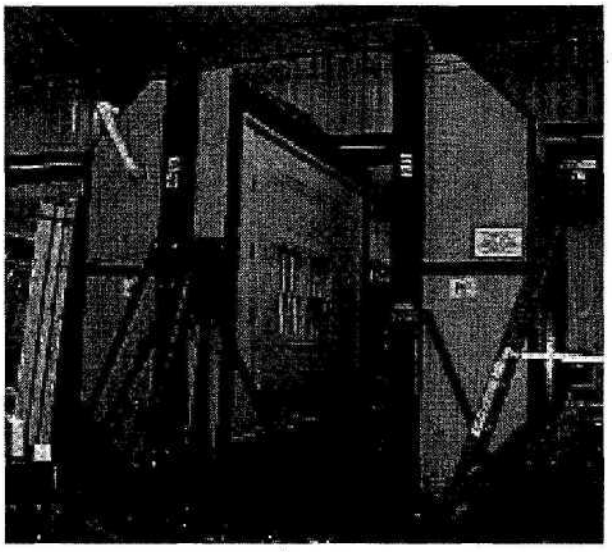

Figure 1 *Rotatable guarded hot box with one of the windows used in this study mounted in the test frame.*

flow measurements were made on two separate 40- to 50-year-old primary windows before and after the addition of a storm window. All measurements were made in a specially modified guarded hot box that can maintain both a temperature and pressure difference across the envelope test specimen.

EXPERIMENTAL APPARATUS

The test assemblies were tested in accordance with *ASTM C 236-89, Steady-State Thermal Performance of Building Assemblies by Means of a Guarded Hot Box* (ASTM 1993), using the ORNL rotatable guarded hot box (RGHB) (Christian and Kosny 1995). A photograph of the device and a schematic are shown in Figures 1 and 2, respectively.

The test assemblies were installed into a specimen frame that is mounted on a movable dolly. The specimen frame has an aperture of 4 by 3 m (13 by 10 ft.). Since the window test assemblies evaluated are smaller than this aperture, the remaining area is filled with a thermally resistive foam insulation material and the thickness of the fill material is adjusted to match the thickness of the test wall assembly. The test specimen assembly is inserted between two chambers of identical cross section. The insertion of the test exterior envelope assembly between the chambers allows the chamber temperatures to be independently controlled. These chambers are designated as the climate (cold) and metering/guard (hot) chambers.

In the climate chamber, a full-size baffle is mounted approximately 250 mm (10 in.) from the test specimen assembly. Temperature control in this chamber is accomplished by the insertion of a refrigeration system and electrical resistance heaters in series with an array of air blowers. An external refrigeration system is operated continuously, and cooled air is transferred from the refrigeration system through insulated flexible duct into the rear of the climate chamber behind the baffle. Five centrifugal air blowers, installed in the climate chamber behind the baffle, are used to circulate the air through a bank of electrical resistance heaters and through the airspace between the baffle and test specimen assembly. Temperature control is accomplished by a combination of controlling the airstream temperature entering the climate chamber and fine-tuning that temperature with the resistance heaters. The air velocity parallel to the climate side of the test specimen assembly is controlled by adjusting the input frequency to the air blowers. An anemometer continuously measures the wind speed in the airspace.

In the center of the metering/guard chamber, a metering box is pressed against the test specimen assembly. The

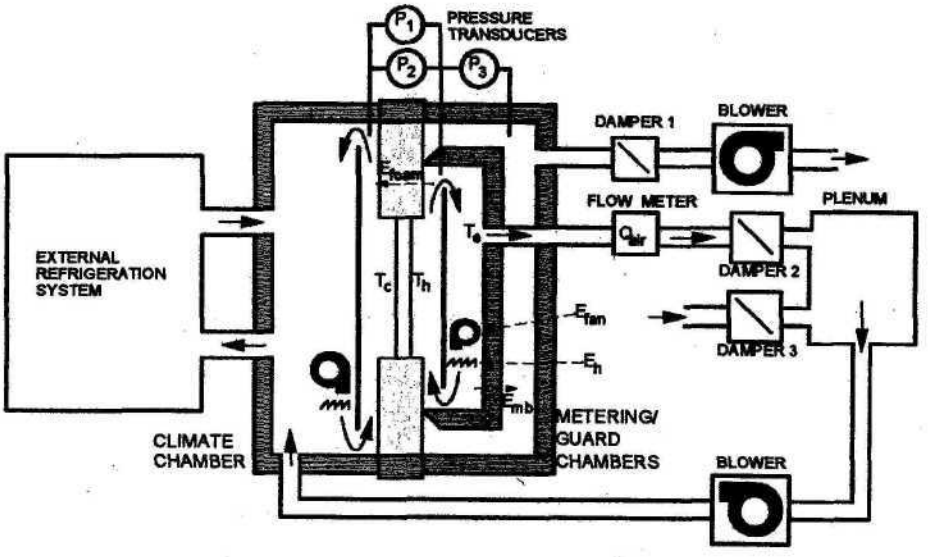

Figure 2 *Schematic of rotatable guarded hot box.*

metering chamber is approximately 2.3 m (8 ft.) square by 0.4 m (1.3 ft.) deep. The walls of the metering chamber are constructed with 76 mm (3 in.) thick, aged extruded polystyrene foam having an approximate thermal resistance of 2.6 $m^2 \cdot K/W$ (15 $h \cdot ft^2 \cdot °F/Btu$) at 24°C (75°F). The walls of the metering box are reinforced with aluminum frames on the interior and exterior sides and are interconnected with fiberglass threaded rods. The edge of the metering chamber that contacts the test assembly is tapered to a thickness of 19 mm (0.75 in.), and a 13 mm (0.5 in.) square neoprene rubber gasket is affixed to this tapered edge. A baffle is mounted inside the metering box 150 mm (6 in.) from the exposed edge of the gasket. Behind the baffle, an array of eight fans and four electric resistance heaters is installed. These components are installed such that air is pulled downward behind the baffle, through the resistance heaters, and upward through the airspace between the baffle and test assembly. The upper and lower rear corners of the metering box are tapered to minimize air impingement onto the metering box walls and to provide a smooth transition into the baffle space.

Four heaters and six fans are installed in the guard box to supply heat and circulate the air. These heaters and fans are situated to uniformly distribute the heat and not impinge directly onto the metering chamber. All of the heat from the heaters and fans is accounted for in the energy balance used to calculated the wall thermal performance.

A 96-junction (48-pair) differential thermopile is applied on the interior and exterior walls of the metering chamber to sense the temperature imbalance between the metering and guard chambers. Each thermopile junction is mounted in the center of equivalent surface areas; the interior junction is mounted directly opposite the corresponding exterior junction. Additional arrays of temperature sensors are affixed to both the meter-side and climate-side surfaces of the foam panel surrounding the test specimen in the area covered by the metering chamber. All of the thermocouples that were attached to the surface of the foam were affixed with cloth duct tape.

Arrays of 36 and 48 thermocouples were used to measure the meter and climate chamber air temperatures. All temperature measurements were performed using type-T copper/constantan thermocouples calibrated to the special limits of error specified in *ASTM E 230, Temperature-Electromotive Force (EMF) Tables for Standardized Thermocouples* (ASTM, no date). All thermocouples were fabricated with No. 26 American wire gauge wire prepared from the same spool of wire.

To create air leakage through the test assembly, a 76 mm (3 in.) diameter port is opened in the metering chamber and a plastic tube is inserted through the opening. A flexible hose is connected to the tube and is passed through the guard chamber wall and connected to a centrifugal blower mounted externally to the hot box. Between the blower and the guard chamber wall, a damper and a 76 mm (3 in.) diameter by 1.8 m (72 in.) long tube are installed. Fifteen tube diameters or 1.1 m (45 in.) upstream of the blower, a hot wire anemometer is mounted to determine the air velocity within the tube. Surveys of the air velocity as a function of radial location are performed and area-weighted to determine the mass flow rate. A second centrifugal blower was connected via flexible hosing to the guard chamber.

Three differential pressure transducers were installed in the rotatable guarded hot box. Two of the transducers, P1 and P2, measure the pressure difference across the test assembly. These two transducers have different pressure ranges. The third transducer, P3, monitors the pressure difference between the metering and guard chambers.

In operation, the temperature of the climate chamber is set at the desired level. A controllable AC source is used to energize the metering chamber heaters, while the metering chamber fans are powered using a programmable D.C. power supply. The power to the fans is fixed to maintain the desired wind speed in the airspace between the baffle and the test wall assembly. An anemometer is used to set and monitor this wind speed. The power to the metering chamber heaters is adjusted to obtain the required metering chamber temperature. The output of a differential thermopile is used to energize the heaters in the guard chamber by using a differential temperature controller. By this technique, the temperature difference across the metering box walls is minimized, thereby permitting negligible heat leaks into or out of the metering chamber.

The test specimen is first tested with zero pressure difference from surface to surface. Then, to induce air leakage through the test specimen, the blower connected to the metering chamber is energized, and the pressure difference across the test assembly is controlled by either adjusting the damper or the speed of the blower. The blower connected to the guard chamber is adjusted to minimize the pressure difference between the metering and guard chambers and, thus, the air leakage either through the metering chamber walls or past the seal between the meter chamber and the test assembly.

These conditions are maintained until temperatures and heat flows and pressure differences equilibrate. The heat flow generated by the heaters is measured using a watt-hour transducer, and the energy dissipated by the fans is metered with precision resistor networks. Once steady-state conditions have been achieved, the test period is continued until two successive four-hour periods produce results that vary nonmonotonically by less than one percent. The data for each period are the average of one-minute scans for that period.

DESCRIPTION OF OPAQUE WALLS AND MEASUREMENTS

The cold formed steel-frame wall system was assembled with 1.1 cm (7/16 in.) orientated strand board sheathing. The boards were installed according to the manufacturer's recommended spacing over a metal flange of 0.3 cm (1/8 in.). The fasteners were on 0.3 m (1 ft) spacing. Fiberglass batt insulation was placed between the 0.4 m (16 in.) on center C-stud

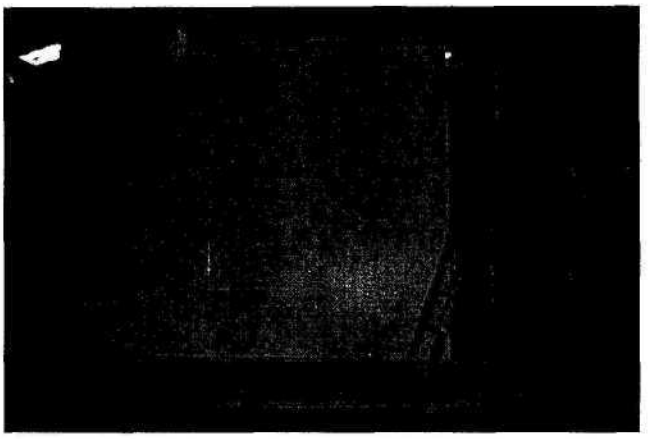

Figure 3 Metal stress skin panel in test frame.

frame wall. A duplex electric outlet with switch was installed in the wall and a conventional electric wire run entirely across the wall through the studs. The insulation was cut at the location of the electric wire and was carefully installed around the wire so that no insulation was compressed. The electrical boxes were not air sealed (as typically installed) and no interior air retarder such as polyethylene was installed prior to finishing the interior surface with gypsum. Airtightness measurements of this wall system revealed surprisingly tight construction.

Even at 75 pascals, no measurable air leakage was recorded. The experimental plan called for application of 1.9 cm (3/4 in.) thick continuous layer of sprayed polyurethane foam within the cavity and 1.3 cm (2 in.) thick layer over the interior metal C-stud flange prior to fiberglass batt insulation installed in the wall cavities and attachment of the interior drywall. This finding suggests that the air-leakage path in this type of wall does not necessarily come through the clear wall but rather through the interface details.

The second opaque wall system, which consisted of metal-faced sandwich panels, had two 2.4 m (8 ft) panel to panel joints. The three panels are assembled in the frame in Figure 3. This wall system was found to permit some air

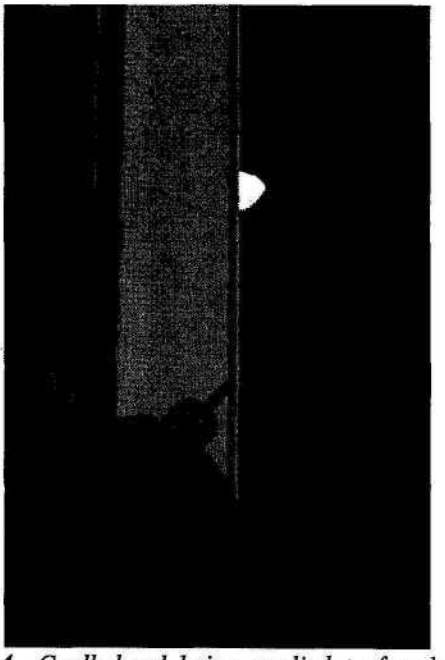

Figure 4 Caulk bead being applied to female vertical edge of panel.

movement through the seams. The lightweight panel had an 0.15 m (6 in.) thick expanded polystyrene insulation core. The panel to panel joint consisted of a male and a female edge. The cold-side metal skin is sealed by a 0.6 cm (1/4 in.) caulk bead placed near the edge of the male edge, which is set into the female edge of the adjacent panel. Figure 4 shows the caulk bead being run on the inside of the metal facing. Three 1.2 m (4 ft) wide panels were used to build the test specimen. Two 2.4 m (8 ft) long seams were placed across the metered area. Thus, the potential air passage through this wall consisted of 4.8 m (16 ft) crack length.

The measurements made on this clear wall test specimen are shown in Figure 5. Two sets of data are shown. In the first data set, no pressure is applied across the wall. The resulting surface-to-surface R-value is 4.4 m^2 k/W (25 h·ft^2·°F/Btu). The impact of pressure of 75 pascals, equivalent to a direct

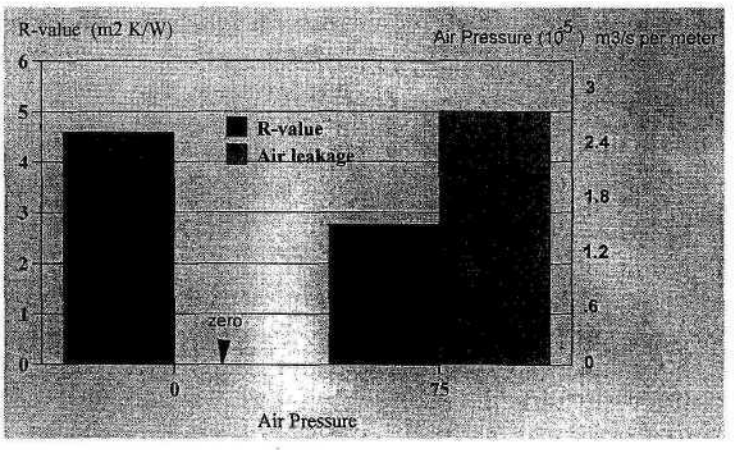

Figure 5 Measurements on clear wall test specimen.

Figure 6 Harvesting Window 1 from the field.

wind speed perpendicular to the wall surface of 6.7 m/s (15 mph), reduces the R-value to 2.6 $m^2 \cdot k/W$ (15 $h \cdot ft^2 \cdot °F/Btu$), represents a 40% drop in R-value. The measured air leakage was 0.56×10^{-3} m^3/s (1.18 cfm), which is 0.03×10^{-3} m^3/s per meter (0.07 cfm per foot) of crack length. The average panel temperature for this test was about 7.2°C (45°F). At room temperature, with no temperature difference across the wall, the measured air leakage was 0.9×10^{-3} m^3/s per meter (2.0 cfm). This suggests that the panel actually tightens at colder temperatures. This is not what was anticipated. Additional pressure conditions are to be applied across this test wall but were not completed in time for the IEA Annex 32 meeting in Scotland on October 28-30, 1997.

DESCRIPTION OF WINDOWS AND MEASUREMENTS

Two windows were evaluated for their heat loss as a function of air leakage with and without the addition of storm windows. Both of the windows were removed from older homes in Knoxville, Tennessee. Figure 6 shows window 1 being removed from one of the houses with a chain saw. The window was removed in this fashion to make sure it was representative of in-situ conditions. The house was habitable up to one month prior to its demise and was taken out of service because the surrounding land was being developed for a planned residential community. Window 1 (Figure 7) was a double-hung window approximately 1.0 m (41 in.) wide by 1.3 m (50 in.) high. The top sash was composed of three lites, while the bottom sash has a single lite. Problems with this window included loose sashes, no weather stripping, gaps between the sashes and frame, missing caulk, cracked glass, and frame dry rot. Window 2 (Figure 8) was a dual double-hung window approximately 1.9 m (75 in.) wide by 1.1 m (42 in.) high. Each sash was fabricated of eight single-glazed lites. This window had loose sashes and no weather stripping. Four tests were conducted for each of these windows with pressure differences across the window ranging from no pressure difference to the maximum pressure difference achievable with the test equipment. The pressure field was not reversed. Only a negative pressure in the metering chamber relative to the climate chamber was maintained.

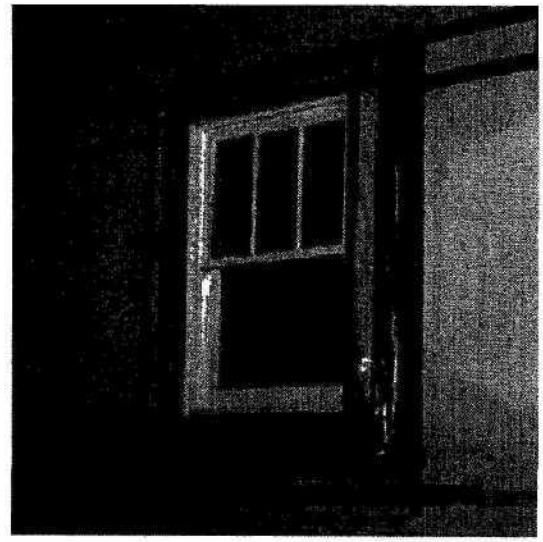

Figure 7 Window 1.

Appropriately sized storm windows for these windows were purchased from a local window supplier. These storm windows were fabricated with a non-thermally broken aluminum frame, had operable sashes, and no weatherstripping. The storm windows were screwed in place around their perimeter and caulked to the surround panel. After installation of storm windows, each of the windows were subjected to four tests with different pressure differences across the window. The pressure differences ranged from zero to the maximum that could be achieved with the test equipment.

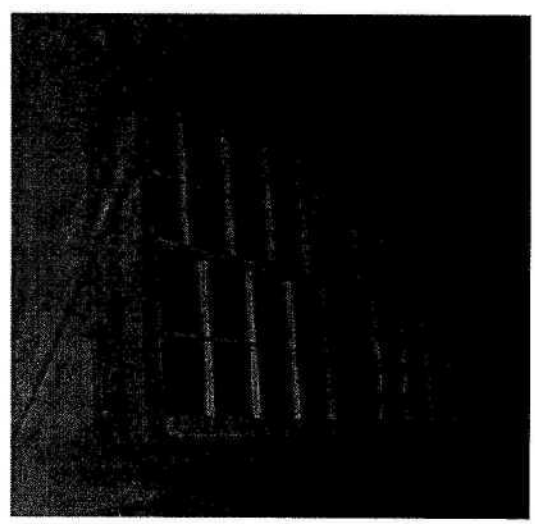

Figure 8 Window 2.

WINDOW DATA ANALYSIS

The metering box energy exchange, E_{mb}, and the energy exchange through the foam, E_{foam}, are calculated in Equations 1 and 2 and shown schematically in Figure 2.

$$E_{mb} = \frac{A_{mb}\Delta_{mb}}{R_{mb}}, \tag{1}$$

and

$$E_{foam} = \frac{A_{foam}\Delta T_{foam}}{R_{foam}}, \tag{2}$$

where

E_{mb} = heat flow through metering box walls, W (Btu/h);

A_{mb} = surface area of the metering box, m^2 (ft^2);

ΔT_{mb} = temperature imbalance across the metering box walls, °C (°F);

R_{mb} = thermal resistance of the metering box walls, m^2·K/W (h·ft^2·°F/Btu);

E_{foam} = heat flow through portion of foam panel surrounding window assembly in the metering area, W (Btu/h);

A_{foam} = surface area of surrounding foam panel in the metering box, m^2 (ft^2);

ΔT_{foam} = temperature difference across surrounding foam panel, °C (°F);

R_{foam} = thermal resistance of the foam measured in accordance with ASTM C 518-91, m^2·K/W (h·ft^2·°F/Btu).

The energy conducted through the window assembly, E_{win}, is calculated for the no-flow condition (i.e., ΔP across the wall is zero) from

$$E_{win} = E_h + E_{fan} - E_{mb} - E_{foam}, \tag{3}$$

where

E_h = energy input to the resistance heaters in the metering chamber, W (Btu/h);

E_f = energy input to the fans in the metering chamber, W (Btu/h).

The overall thermal resistance of the window assembly is calculated from

$$R_{win} = \frac{A_{win}(T_h - T_c)}{E_{win}}, \tag{4}$$

where

R_{win} = overall thermal resistance of window assembly, m^2·K/W (h·ft^2·°F/Btu);

A_{win} = area of window, m^2 (ft^2);

T_h = average metering-side air temperature measured 76 mm (3 in.) from surface of test specimen, °C (°F);

T_c = average climate-side air temperature measured 76 mm (3 in.) from surface of test specimen, °C (°F).

The procedure described above is also used for the tests with a pressure difference across the window except that the energy associated with the window calculated in Equation 3 is due predominately to two heat transfer mechanisms, a conduction component and an air infiltration component, rather than just conduction. The air infiltration component can be calculated from

$$E_{air} = E_{win} - E_{cond}, \tag{5}$$

where

E_{air} = energy exchange due to air infiltration, W (Btu/h);

E_{cond} = heat conducted through the glazing and frame of the window, W (Btu/h).

The heat conducted through the glazing and frame of the window is calculated as

$$E_{cond} = \frac{A_{win}(T_h - T_c)}{R_{win}(\Delta P = 0)}, \tag{6}$$

where

$R_{win(\Delta P=0)}$ is the window overall R-value determined from a measurement with zero pressure difference across the window.

The energy exchange due to air infiltration, E'_{air}, can also be calculated from the measured flow rate of air being drawn from the metering chamber:

$$E'_{air} = Q_{air}\rho c_p(T_e - T_c) \tag{7}$$

where

Q_{air} = measured volumetric flow rate of air leaving metering chamber, m^3/s (ft^3/min);

ρ = air density, kg/m^3 (lbm/ft^3);

c_p = air specific heat, J/kg·K (Btu/lbm·°F);

T_e = air temperature exiting metering chamber, °C (°F).

However, data from tests (discussed later in this paper) indicate that the energy transfer due to infiltration calculated with Equation 7 is consistently lower than that calculated with Equation 5 for all cases, with the difference ranging from 12% to 22%. This suggests that the influence of infiltration on energy flow is more than just the energy needed to raise the temperature of the air leaking through the window. This was found to be consistent with test results from the metal sandwich wall as well. The difference was found to be 12.9%, as shown in the last row of data in Table 1. It is speculated that the air infiltration alters the local temperature distribution in the vicinity of the leakage path and, thus, the conductive heat transfer. For example, in winter conditions with air infiltration at a window, portions of the window sash/frame near the interior surface may be exposed to the outside air temperature. This has the effect of shortening the conduction path from outside to inside, resulting in a lower effective overall R-value and higher heat transfer rate.

TABLE 1
Window Data

Window	Measurements				Eqn. 3	Eqn. 8	Eqn. 9	Eqn. 10	Eqn. 11	Eqn. 12
	ΔP	$T_h - T_c$	$T_e - T_c$	Q_{air}	E_{win}	E'_{win}	E''_{win}	E_{air}	Q_{eff}	q_{eff}
	Pa (psi)	°C (°F)	°C (°F)	m^3/s (ft^3/min)	W (Btu/h)	W (Btu/h)	W (Btu/h)	W (Btu/h)	m^3/s (ft^3/min)	$m^3/s \cdot m$ ($ft^3/min \cdot ft$)
1	4.06 (5.89×10^{-4})	25.1 (45.2)	23.8 (42.8)	6.772×10^{-3} (14.35)	323.4 (1103.4)	333.7 (1138.6)	369.1 (1259.5)	274.3 (936.1)	8.641×10^{-3} (18.31)	1.527×10^{-3} (0.986)
	7.56 (1.10×10^{-3})	25.7 (46.3)	24.3 (43.8)	$1.021\cdot10^{-2}$ (21.64)	478.5 (1632.8)	494.7 (1688.1)	534.3 (1823.0)	439.5 (1499.6)	1.385×10^{-2} (29.34)	2.445×10^{-3} (1.579)
	8.53 (1.24×10^{-3})	26.7 (48.1)	25.4 (45.7)	1.210×10^{-2} (25.63)	562.9 (1920.7)	581.7 (1984.9)	604.7 (2063.3)	509.9 (1739.9)	1.607×10^{-2} (34.04)	2.837×10^{-3} (1.832)
1+Storm	9.37 (1.36×10^{-3})	27.7 (49.9)	28.7 (51.7)	$2.218\times10^{-}$ (4.70)	144.9 (494.4)	142.4 (485.8)	142.6 (486.7)	87.2 (297.5)	2.747×10^{-3} (5.82)	4.846×10^{-4} (0.313)
	22.50 (3.26×10^{-3})	25.6 (46.1)	25.4 (45.8)	4.776×10^{-3} (10.12)	236.9 (808.3)	237.8 (811.4)	257.9 (880.0)	202.5 (690.8)	6.376×10^{-3} (13.51)	1.126×10^{-3} (0.727)
	42.20 (6.12×10^{-3})	22.9 (41.2)	21.8 (39.3)	8.141×10^{-3} (17.25)	290.8 (992.2)	300.6 (1025.7)	364.8 (1244.8)	309.4 (1055.6)	9.746×10^{-3} (20.65)	1.720×10^{-3} (1.111)
2	4.50 (6.53×10^{-4})	25.6 (46.1)	25.2 (45.4)	9.557×10^{-3} (20.25)	566.7 (1933.8)	570.8 (1947.5)	619.6 (2114.1)	441.3 (1505.9)	1.390×10^{-3} (29.46)	1.496×10^{-3} (0.966)
	6.25 (9.06×10^{-4})	24.6 (44.2)	24.9 (44.9)	1.194×10^{-2} (25.29)	685.2 (2338.0)	680.0 (2320.4)	768.9 (2623.7)	590.7 (2015.6)	1.861×10^{-2} (39.43)	2.002×10^{-3} (1.293)
	11.56 (1.68×10^{-3})	23.4 (42.2)	23.2 (41.7)	1.633×10^{-2} (34.61)	802.77 (2739.0)	808.2 (2757.8)	956.9 (3265.2)	778.7 (2657.0)	2.453×10^{-2} (51.98)	2.638×10^{-3} (1.704)
2+Storm	13.00 (1.89×10^{-3})	23.7 (42.7)	23.6 (42.5)	7.683×10^{-3} (16.28)	363.3 (1239.5)	364.2 (1242.7)	426.2 (1454.1)	331.8 (1132.1)	1.045×10^{-3} (22.15)	1.124×10^{-3} (0.726)
	20.81 (3.02×10^{-3})	23.1 (41.5)	23.3 (42.0)	1.150×10^{-2} (24.36)	507.0 (1729.8)	503.4 (1717.6)	606.2 (2068.4)	511.8 (1746.5)	1.612×10^{-2} (34.16)	1.734×10^{-3} (1.120)
	29.06 (4.21×10^{-3})	22.1 (39.8)	22.2 (40.0)	1.412×10^{-2} (29.92)	564.2 (1925.0)	562.7 (1920.1)	706.9 (2412.2)	612.6 (2090.2)	1.930×10^{-2} (40.89)	2.076×10^{-3} (1.341)

Even though infiltration influences the conduction, it is desirable to develop a model that leaves the conduction portion alone but adds an infiltration term that accounts for both the direct infiltration heat flow and the effect infiltration has on conduction. To do this, an effective airflow rate is calculated (i.e., the flow rate necessary to account for the difference in energy flow between the no-flow conduction and the measured total).

The air exiting the metering chamber, T_e, is generally at a lower temperature than the average air temperature in the metering chamber, T_h, because it is not resident in the chamber long enough to come to equilibrium with the chamber air. The difference between T_h and T_e increases with increasing air infiltration. The amount of energy, E'_{win}, needed to change the temperature of the exiting air to the average metering chamber air temperature is calculated and added to the measured energy input to the metering chamber to correct for this.

$$E'_{win} = E_{win} + Q_{air}\rho c_p(T_h - T_e) \tag{8}$$

Since the temperature difference across the window varies from test to test, the energy input to the metering chamber is corrected to a standardized temperature difference, ΔT_{std}, of 27.8°C (50°F).

$$E''_{win} = E'_{win}\frac{\Delta T_{std}}{(T_h - T_c)} \tag{9}$$

The portion of the energy due to the infiltration effects is determined by subtracting the standardized conduction portion from the total.

$$E_{air} = E''_{win} - \frac{A_{win}\Delta T_{std}}{R_{win}} \tag{10}$$

An effective volumetric flow rate, Q_{eff}, is then calculated (i.e., the flow rate that is required for the simple conduction-plus-infiltration model to give the correct energy flow).

$$Q_{eff} = \frac{E_{air}}{\rho c_p(T_h - T_c)} \tag{11}$$

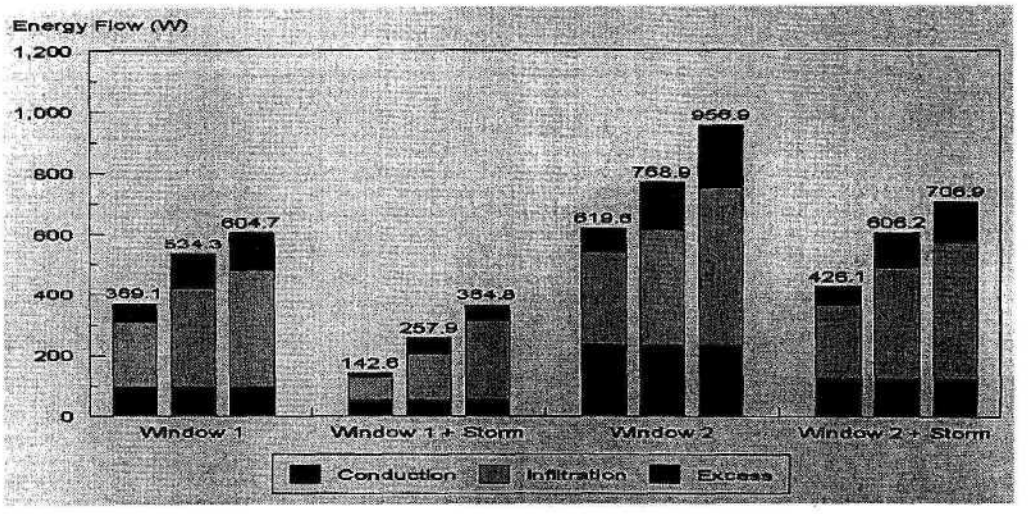

Figure 9 *Energy flow through window assemblies.*

Finally, an effective volumetric flow rate per meter (foot) of crack length, q_{eff}, is calculated to make the results more applicable to windows of different size.

$$q_{eff} = \frac{Q_{eff}}{L_c} \tag{12}$$

where, for a double-hung window,

$$L_c = 3W + 2H \tag{13}$$

and

W = window width, m (ft);

H = window height, m (ft).

Experimental data and results from the calculations described above are presented in Table 1. A different representation of these same data is presented in Figure 9. The bottom portion of each bar is the conductive heat flow calculated with the standardized temperature difference and the R-value determined with no pressure difference across the window. The middle portion of each bar is the heat flow directly attributable to infiltration and is calculated using the measured flow rate and the standardized air temperature change. The top portion of each bar is the excess heat flow not accounted for by the normal conduction plus infiltration model. The entire height of each bar represents the measured total energy flow through the window assembly corrected to the standardized temperature difference, E''_{win}.

METHODOLOGY

This section outlines a methodology for taking data from hot box tests and deriving a simple calculational technique. This section is a theoretical discussion that does not make use of the data discussed in the previous section. After the methodology has been presented in this section, the hot box data will be used with the methodology in the following section.

It is expected that the volumetric airflow rate will vary with pressure difference according to the power law equation (ASHRAE 1997),

$$Q = a(\Delta P)^N \tag{14}$$

where

a = flow coefficient, $m^3/s \cdot Pa^N$ ($ft^3/min \cdot psi^N$);

N = flow exponent, dimensionless.

The values for a and N are constants for a particular type of exterior envelope. Furthermore, it is speculated that there is a value for N that is characteristic of window air leakage in general and possibly exterior envelope clear wall and interface details (corner, wall/ceiling, wall floor, window surround, door surround). Of course, measurements will need to be made on additional windows and opaque envelope clear wall and interface details to confirm this speculation and to determine a suitable value for N. The a term is characteristic of a particular window or opaque envelope detail and represents the leakiness of the envelope component—the higher the value, the leakier the component. The constants a and N will be determined by doing least squares fits of the effective flow rate vs. pressure difference data from pressurized hot box tests.

For any particular envelope component, data from a series of pressurized hot box tests can be used to determine the constant a_P. After a storm window or air leakage control provision is added, data from another series of pressurized hot box tests can be used to determine the constant a_{P+S} for the primary/storm or opaque detail/air control assembly. For example, the installation of a storm window over a primary window places an additional resistance to airflow in series with the resistance due to the primary window. The airflow through the storm window is the same as the airflow through the primary window since all other flow paths have been sealed for the test; thus,

$$a_P(\Delta P_P)^N = a_S(\Delta P_S)^N = a_{P+S}(\Delta P)^N = Q. \tag{15}$$

The total pressure difference across the primary/storm window assembly is equal to the sum of the pressure difference across the storm window and the pressure difference across the primary window.

$$\Delta P_P + \Delta P_S = \Delta P \tag{16}$$

The values of a_P and a_{P+S} are already know from the curve fit of data from hot box experiments, and a_S can be determined from Equations 15 and 16 as

$$a_S = \left[\frac{1}{\left(\frac{1}{a_{P+S}}\right)^{\frac{1}{N}} - \left(\frac{1}{a_P}\right)^{\frac{1}{N}}} \right]^N \tag{17}$$

The measurements and calculations just described give a value of the flow coefficient for one particular quality of primary window and one particular quality of storm window. These values will be entered into Tables 2 and 3. Envelope descriptions in these tables must be detailed and clear enough to allow someone in the field to readily match a window in a house to one of the categories in the table. The categories and descriptions will evolve as more windows are tested.

Opaque wall air sealing techniques can be represented in a similar fashion, as shown in Table 4, for storm windows. Opaque wall air-tightening enhancements would be caulk and seal, house fabric wrap, airtight insulation (i.e., spray foam), etc.

Once the tables have been filled in either by additional measurements or interpolation between measurements, they can be used to determine the effectiveness of adding a particular class of storm window to a particular primary window or air control provision to a type of opaque wall system. Values of a_P and a_S are selected from Tables 2 and 3, respectively. The leakage per unit length of crack for the primary window or base opaque is given by

$$q_P = a_P(\Delta P)^N, \tag{18}$$

and the leakage per unit length of crack for the primary window plus a storm window or opaque envelope plus air control provision is given by

$$q_{P+S} = a_{P+S}(\Delta P)^N, \tag{19}$$

where a_{P+S}, the flow coefficient for the primary window plus the storm window or opaque envelope plus air control provision, is calculated as

$$a_{P+S} = \frac{1}{\left(\frac{1}{a_P}\right)^{\frac{1}{N}} + \left(\frac{1}{a_S}\right)^{\frac{1}{N}}}. \tag{20}$$

Thus, the reduction in airflow attributable to the addition of the storm window or other air control provision is

TABLE 2
Storm Window Selections

Description	a_S
Low-cost storm window. No weatherstripping.	
With weatherstripping.	
Non-movable sash.	

TABLE 3
Primary Window Selections

Description	a_P
Very leaky window. Loose sash. Cracks wide enough to see light through.	
Leaky.	
Good.	

TABLE 4
Best Individual Curve Fits for Each of Four Test Series

	a		N
Window ID	**$m^3/s \cdot m \cdot Pa^N$**	**$ft^3/min \cdot ft \cdot psi^N$**	**dimensionless**
Window 1	4.89H10^{-4}	406.3	0.81
Window 1 with storm	7.62×10^{-5}	82.5	0.84
Window 2	5.11×10^{-4}	103.2	0.65
Window 2 with storm	1.24×10^{-4}	122.9	0.83

$$\Delta q_S = (a_{P+S} - a_P)(\Delta P)^N. \tag{21}$$

Generally simplified tools account for energy savings due to a reduction in conduction with the addition of the storm window. The use of Tables 2 and 3, along with Equations 20 and 21, offers an easy method to account for energy savings due to the reduction of infiltration with the addition of a storm window. On a whole house basis, infiltration predictions prior to construction are +100%. Itemizing the predominant potential air leakage passages offers an opportunity to improve the predictability of airtightness prior to retrofit or new construction.

IMPLEMENTATION OF METHODOLOGY USING THE WINDOW DATA

The data from the four test series (window 1 without storm, window 1 with storm, window 2 without storm, and window 2 with storm) are used to determine if the methodology outlined in the previous section is valid. The main points that need to be verified are:

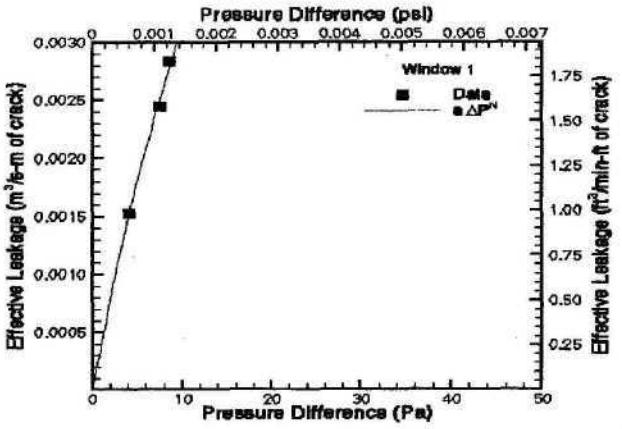

Figure 10 *Leakage for Window 1.*

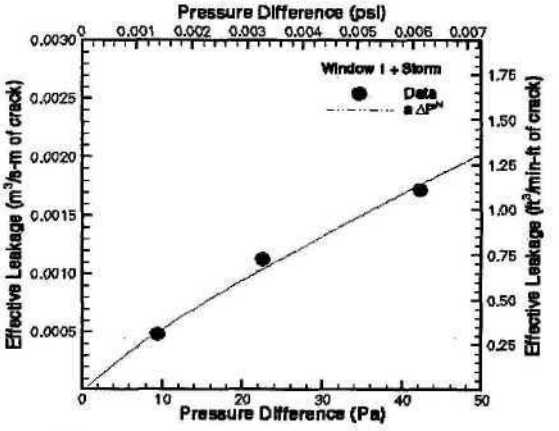

Figure 11 *Leakage for Window 1 with storm.*

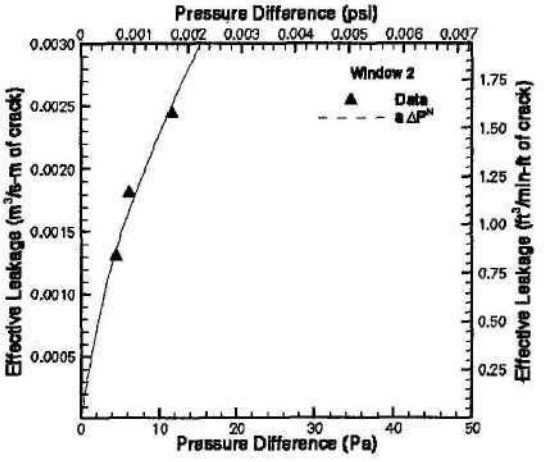

Figure 12 *Leakage for Window 2.*

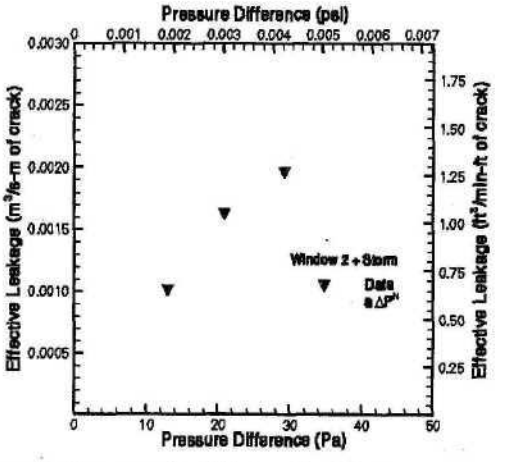

Figure 13 *Leakage for Window 2 with storm.*

- Does the power-law equation adequately represents the observed window leakage behavior?,
- Is there a unique power term, N, that adequately characterizes flow through windows in general?,
- Is there a flow coefficient, a, that is characteristic of a particular type of window and, once determined, can it be used to calculate leakage through the window individually or through the window in series with another window?

Least-squares fits minimizing the sum of squares of the relative differences between measured and predicted flows were performed individually for each of the four test series. Both N and a were determined from these fits. Results from these fits are shown in Figures 10 through 13 and in Table 4.

The flow exponent N is essentially the same for three of the window configurations tested. The one outlier is Window 2 without a storm window. A couple of possible explanations for this behavior have been identified. First, the test equipment used was not capable of producing large pressure differences across the window, which resulted in all three data points having a fairly narrow range of pressure difference. Second, a visual examination of the window after the tests identified an additional air leakage path at the mulling joint (where the edges of the two windows meet). The intent was to eliminate all leakage paths except those around the window sash. It is not clear how this additional leakage path skews the results. A dual window arrangement has the potential for greater air infiltration than the sum of the individual windows. This suggests that, for new construction, extreme care is needed to durably seal between mulled (ganged) windows.

Next, data from all four of the test series are used collectively in a least-squares fit to determine a single value of N that best represents all of the data and a value of a for each series. The results are shown in Figure14 and Table 5. The common power term of $N = 0.8$ seems to reasonably model the observed behavior of all of the test series and is used to develop the curves in Figure 14. Even for Window 2, the fit visually appears to be as good as the stand-alone fit (for which $N = 0.65$).

The 1992 *Model Energy Code* Compliance Guide states that the maximum leakage rate at a pressure difference of 75.0 Pa (1.576 lb/ft^2) is 5.26×10^{-4} m^3/s·m of operable sash

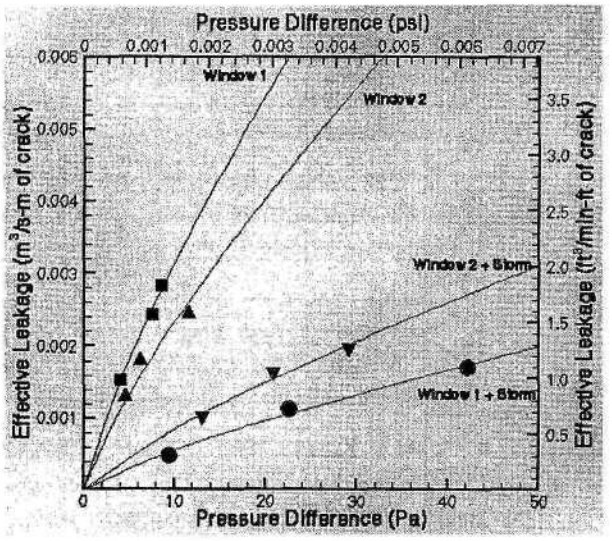

Figure 14 Leakage for all window assemblies.

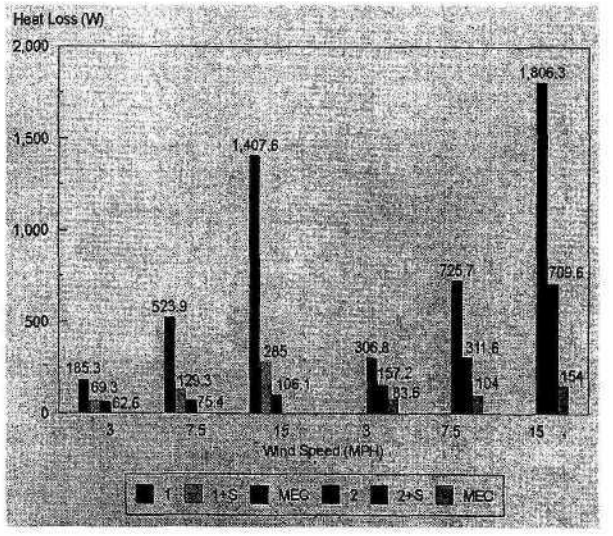

Figure 15 Heat loss for window assemblies at various wind speeds.

TABLE 5
Best Curve Fit for
All Four Test Series Collectively

Window ID	a		N
	$m^3/s \cdot m \cdot Pa^N$	$ft^3/min \cdot ft \cdot psi^N$	dimensionless
Window 1	4.99×10^{-4}	379.0	0.80
Window 1 with storm	8.76×10^{-5}	66.6	
Window 2	3.69×10^{-4}	280.2	
Window 2 with storm	1.36×10^{-4}	103.7	
MEC-compliant Window	1.66×10^{-5}	12.7	

crack (0.34 ft^3/min·ft of operable sash crack). This data point can be used to determine the flow coefficient, a_{MEC}, in the power law equation for a MEC-compliant window. For comparison, this value is also included in Table 5. The value for a_{MEC} only accounts for direct infiltration and not for any impact infiltration may have on conduction; but, since infiltration is low for a MEC-compliant window, the impact on conduction is also expected to be minor.

Figure 15 shows the heat loss for each of the tested window configurations for a 27.8°C (50°F) temperature difference and three different wind speeds. For comparison, an MEC-compliant window of the same size is included. Pressure differences across the window are calculated by assuming that the window is facing directly into an unobstructed wind at the specified velocity. The pressure difference will be less for a window not facing directly into the wind or a window protected from the wind. The implementation into whole building energy simulation models will have to make allowances for these situations.

Equation 17 is used to calculate the flow coefficients for the storm windows applied to Window 1 and Window 2. The values of a_s for the storm windows added to Window 1 and Window 2 are 0.0624 and 0.1156, respectively. These values indicate that the storm window added to Window 2 is much leakier than the storm window added to Window 1. This is readily apparent in Figure 14, where it can be seen that Window 1 is much leakier than Window 2; but, after adding storm windows to both, Window 1 becomes much tighter than Window 2. However, since both storm windows have the same basic construction, they should have the same flow coefficient. The previously identified additional leakage path for Window 2 may be a partial explanation for this behavior, but it is not clear if this is the sole reason for the unexpected behavior.

CONCLUSIONS AND FUTURE WORK

A methodology has been proposed for quantifying the reduction in infiltration brought about by the addition of a storm windows but also potentially expandable to airtightness control provisions for both windows and opaque walls. Tests conducted on two window systems with and without storm windows were used to test the methodology. Due to the limited variety of windows tested, it is not possible to come to a definite conclusion about the universal applicability of the method. It will be necessary to test additional windows in order to confirm, refute, or modify the method and to collect sufficient data to implement it into existing software tools. In addition to a need to test many more types of primary windows, it is necessary to test different storm windows and different air leakage reduction strategies. Another issue that needs to be addressed is the economic trade-off of repairing a faulty window versus adding a storm window. It is hypothesized that the methodology can be extended to cover opaque wall details. However, even at 75 pascals, no measurable air leakage was recorded in a flat

metal wall panel tested during this project. The experimental plan called for application of a 1.9 cm (3/4 in.) thick continuous layer of sprayed polyurethane foam within the cavity and a 1.3 cm (2 in.) thick layer over the interior metal C-stud flange prior to fiberglass batt insulation installed in the wall cavities and attachment of the interior drywall. This finding suggests that the air-leakage path in this type of wall does not necessarily come through the clear wall but rather through the interface details. If test panels can be made representative of field conditions, this will provide a measurement-based procedure for predicting airtightness during the conceptual stages of building design or retrofit. This was identified by IEA Annex 32 in an April 1997 meeting at Oak Ridge as a major gap in the available tools for verifying the functional requirement C 4.2 airtightness of the building envelope (Integral client's brief, functional descriptions, September 1997).

REFERENCES

ASHRAE. 1997. *1997 ASHRAE Handbook—Fundamentals*. Atlanta: American Society of Heating, Refrigerating and Air-Conditioning Engineers, Inc.

ASTM. *ASTM E 230, Temperature-electromotive force (EMF) tables for standardized thermocouples*. Philadelphia: American Society for Testing and Materials.

ASTM. 1993. *C236-80 (Reapproved 1993), Standard test method of steady-state thermal performance of building assemblies by means of a guarded hot box*. Philadelphia: American Society for Testing and Materials.

Christian, J.E., and J. Kosny. 1995. Toward a national opaque wall rating label. *Thermal Performance of the Exterior Envelopes of Buildings VI*. Atlanta: American Society of Heating, Refrigerating and Air-Conditioning Engineers, Inc.